C. R. Mecanique 345 (2017) 301–316

Contents lists available at ScienceDirect

Comptes Rendus Mecanique

www.sciencedirect.com

Acoustical scattering identification with local impedance through a spectral approach

Mohamed Amine Ben Souf [a,b,*], Ahmed Kessentini [a,b], Olivier Bareille [b], Mohamed Taktak [a], Mohamed N. Ichchou [b], Mohamed Haddar [a]

[a] *Mechanics, Modelling and Production Laboratory (LA2MP), National School of Engineers of Sfax, University of Sfax, BP 1173, Sfax 3038, Tunisia*

[b] *Laboratoire de tribologie et dynamique des systèmes (LTDS), École centrale de Lyon, 36, avenue Guy-de-Collongue, 69134 Écully cedex, France*

ARTICLE INFO

Article history:
Received 24 October 2016
Accepted 18 March 2017
Available online 14 April 2017

Keywords:
Wave finite element
Acoustical propagation
Micro-perforated plate
Locally reacting lining
Scattering

ABSTRACT

Acoustical scattering in waveguides is studied in this paper. The Wave Finite Element (WFE) approach is mainly used, since it allows the reduction of problems dealing with periodic waveguides. The paper deals with guided acoustical propagation, that is, propagation in a main direction is privileged. The scattering by a locally reacting lining is first studied. The liner can be characterised by its local impedance in this case. The equivalent surface impedance is therefore calculated. Then, scattering by a porous layer is considered. A full three-dimensional modelling of the lining is preferred since porous materials are bulk reacting. The scattering matrix of the lined part is computed, and acoustical scattering of high-order modes and conversion between modes are highlighted. The acoustic power attenuation is further evaluated. The response of ducts subjected to constraining boundary conditions is also calculated. Numerical results are presented and compared to those obtained with conventional approaches.

1. Introduction

Reducing noise levels has been one of the main topics dealt with in acoustics. The most standard and readily recognisable technique is to use liners composed essentially of an acoustically absorbing material. However, different liner configurations can be used, depending on the engineering application. The frequency dependence of the acoustic impedance of the liner, and the geometrical characteristics of the liner, which contribute to the expression of the impedance, must be taken into consideration when computing the scattering matrix and the acoustic power attenuation. Different approaches dealt with the acoustic problems using analytical formulations based on the resolution of the Helmholtz equation for canonic examples, or numerical approaches such as Semi-Analytical Finite Element (SAFE) and conventional Finite Element (FE) methods. The Wave Finite Element (WFE) method deals with periodic media. This formulation was firstly developed for photonics [1] and crystal lattice [2] problems. Then, Zhong and Williams [3] extended it for periodic elastic media. The WFE method has been widely used for structural applications: vibrations of uniform waveguide structures [4], Structural Health Monitoring (SHM) and Non-Destructive Testing (NDT) of pipelines [5,6], forced response with harmonic and general load [7], dynamic

* Corresponding author.
E-mail address: bensouf.mohamedamine@gmail.com (M.A. Ben Souf).

http://dx.doi.org/10.1016/j.crme.2017.03.006
1631-0721/

problems of homogeneous thin-walled structures [8], wave propagation in beam-like structures [9], laminates [10], fluid-filled pipes [11], tyres [12] and poroelastic media [13]. The method does not have limitations for the type of element used for modelling. Nevertheless, it may be prone to ill-conditioning issues [14]. Indeed, the cross-sectional mesh density can be raised so that the wave basis is expanded with high-order modes, but time-consuming matrix inversions and ill-conditioned matrices have to be handled while increasing the number of degrees of freedom. For instance, some authors kept only a reduced wave basis while computing the forced response, and the strongly evanescent modes were neglected [15]. The WFE approach was later used for 2D structural applications [16], prediction of the vibro-acoustic behaviour of honeycomb panels [17]. Ben Souf et al. [18] extended the application of the method to media with uncertain parameters and their impact on spectral results.

The scattering matrix can be seen as a characterisation of a lined duct independently of the upstream and downstream conditions [19]. Many works, based on analytical or numerical approaches, focused on the determination of the scattering matrix. Some works, e.g., [20] and [21], used analytical formulations for the computation of the scattering matrix for acoustic problems. In these works, the liner's impedance was assumed to be constant along the duct, and could arbitrarily vary along the circumference. A projection over a rigid duct basis of orthogonal functions was used and terms of coupling between modes due to the scattering were added. Due to the analytical methods constraints, particularly when the geometry is complex, numerical methods were alternatively adopted [22]. These works used a Finite Element method. The scattering matrix of a lined duct was computed for a frequency range such as only uncoupled modes are cut-on, as experiments to extract the acoustic impedance using a pressure source composed of the cut-on modes had to be carried out. In this paper, the WFE method will be used for the rigid parts, and then exploited for computing the acoustical scattering matrix of lined ducts. One elementary cell of the periodic medium is considered. FE commercial packages are used to obtain the mass and the stiffness matrices of the cell. Using the periodicity of the studied medium, a spectral formulation can be written and solved to obtain the wave's characteristics (wavenumbers and deformed shapes). This allows a fairly lower computational cost than when the full FE model is used. The identification of the scattering matrix is based on the hybridisation between the WFE and FE approaches [23], since the lined part of the medium is treated by the conventional FE method. The continuity conditions at the right-hand and the left-hand sides of the coupling element corresponding to the lined part lead to the expression of the scattering matrix.

A well-known solution for reducing noise levels is the use of honeycomb structures. These are particularly used in aircraft engines. The lining is locally reacting and the damping effect can be accurately described by an equivalent impedance at the surface of the duct, that is, simple addition of the acoustic surface impedance of cavities and the acoustic impedance of an associated perforated plate, as detailed in [24–26]. In other engineering applications, porous absorbers can be also used, since they are less frequency dependent. However, it is more convenient to model the entire porous domain rather than using the resulting effective impedance of the wall, as acoustic waves travel also parallel to the walls and an equivalent surface impedance can be only calculated per mode of propagation.

This paper is an extension of the WFE applications to the acoustical guided propagation, and scattering in the presence of acoustic impedance or medium discontinuities. Therefore, different liner configurations are considered. The scattering matrix of the lining is fully calculated considering both propagative and evanescent waves and their conversion. Then, the response of two coupled periodic waveguides with any prescribed boundary conditions (e.g., pressure or velocity excitations, anechoic or partially reflective ends, PML layers...) can be calculated, as well as for single periodic waveguides. An hybrid WFE–FE method can be used while using three-dimensional modelling of the lined part. The considerable advantages of the use of the WFE alternative are reviewed, and the periodicity of the duct parts for which acoustic fields are determined by the WFE method is most likely the only restricting hypothesis of the method.

Notes on the WFE method, empirical models of the acoustic impedance of perforated plates, equivalent fluid theory, and calculation of the acoustic power attenuation are presented in section 2. Numerical examples are dealt with in section 3: Ducts with locally reacting lining are first considered. The effect of the geometric parameters of the liner on the efficiency of the liner is shown. Then, ducts with bulk reacting lining are studied. The considered examples are finally discussed.

2. Theoretical background

2.1. The WFE formulation

The first step of the WFE method is to model a segment of a periodic waveguide, with a same distribution of nodes on its left and right sides, as shown in Fig. 1, say n_{d} degrees of freedom. The FE packages can be used for modelling. The internal nodes are removed using dynamic condensation. The segment length Δ should be chosen such it is at least six times shorter than the minimal wavelength [14,27]. This segment is governed by the equation:

$$\left(-\omega^2 \boldsymbol{M} + \boldsymbol{K}\right) \boldsymbol{p} = \boldsymbol{D}\boldsymbol{p} = \boldsymbol{v} \tag{1}$$

where $\boldsymbol{p}$ and $\boldsymbol{v}$ are respectively the pressures and particle velocities of the nodes, ω is the angular frequency, and $\boldsymbol{M}$ and $\boldsymbol{K}$ are respectively the mass and stiffness matrices of the segment. Eq. (1) can be rewritten as follows:

$$\begin{pmatrix} \boldsymbol{D}_{\mathrm{ll}} & \boldsymbol{D}_{\mathrm{lr}} \\ \boldsymbol{D}_{\mathrm{rl}} & \boldsymbol{D}_{\mathrm{rr}} \end{pmatrix} \begin{pmatrix} \boldsymbol{p}_{\mathrm{l}} \\ \boldsymbol{p}_{\mathrm{r}} \end{pmatrix} = \begin{pmatrix} \boldsymbol{v}_{\mathrm{l}} \\ \boldsymbol{v}_{\mathrm{r}} \end{pmatrix} \tag{2}$$

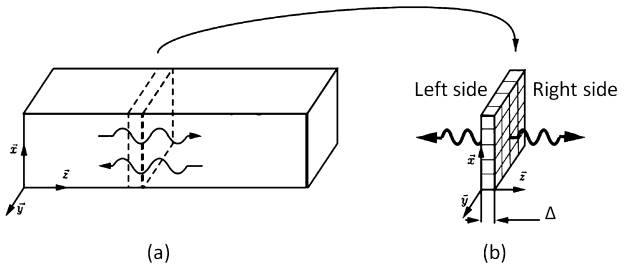

Fig. 1. Schematic of a periodic waveguide (a) and a meshed elementary cell (b).

Subscripts l and r refer to the left- and right-hand sides, respectively. The left and right nodal degrees of freedom are related by a propagation constant λ, as follows:

$$\boldsymbol{p}_{\mathrm{r}} = \lambda \boldsymbol{p}_{\mathrm{l}} \tag{3}$$

$$\boldsymbol{v}_{\mathrm{r}} = -\lambda \boldsymbol{v}_{\mathrm{l}} \tag{4}$$

Eqs. (2), (3) and (4) lead to:

$$\boldsymbol{S}\begin{pmatrix} \boldsymbol{p}_{\mathrm{l}} \\ -\boldsymbol{v}_{\mathrm{l}} \end{pmatrix} = \lambda \begin{pmatrix} \boldsymbol{p}_{\mathrm{l}} \\ -\boldsymbol{v}_{\mathrm{l}} \end{pmatrix} \tag{5}$$

with

$$\boldsymbol{S} = \begin{pmatrix} -\boldsymbol{D}_{\mathrm{lr}}^{-1}\boldsymbol{D}_{\mathrm{ll}} & -\boldsymbol{D}_{\mathrm{lr}}^{-1} \\ \boldsymbol{D}_{\mathrm{rl}} - \boldsymbol{D}_{\mathrm{rr}}\boldsymbol{D}_{\mathrm{lr}}^{-1}\boldsymbol{D}_{\mathrm{ll}} & -\boldsymbol{D}_{\mathrm{rr}}\boldsymbol{D}_{\mathrm{lr}}^{-1} \end{pmatrix} \tag{6}$$

$\boldsymbol{S}$ is a $2n_{\mathrm{d}} \times 2n_{\mathrm{d}}$ matrix.

The problem given by Eq. (5) is solved for each frequency. Pairs of eigenvalues λ_j^{inc} and λ_j^{ref} and corresponding eigenvectors $\boldsymbol{\phi}_j^{\mathrm{inc}}$ and $\boldsymbol{\phi}_j^{\mathrm{ref}}$ are obtained, as with each eigenvalue λ_j^{inc} $(j = 1, \ldots, n_{\mathrm{d}})$ can be associated an eigenvalue $\lambda_j^{\mathrm{ref}} = 1/\lambda_j^{\mathrm{inc}}$. $\left\{\lambda_j^{\mathrm{inc}}\right\}$ are such that $|\lambda_j| < 1$ and correspond to the forward going waves, and $\left\{\lambda_j^{\mathrm{ref}}\right\}$ are such that $|\lambda_j| > 1$ and correspond to the backward going waves. It is useful to consider a reformulation leading to a quadratic eigenproblem which is better-conditioned than problem (5) [14]:

$$\begin{pmatrix} \boldsymbol{0} & \boldsymbol{I}_{n_{\mathrm{d}}} \\ -\boldsymbol{D}_{\mathrm{lr}}^{-1}\boldsymbol{D}_{\mathrm{rl}} & -\boldsymbol{D}_{\mathrm{lr}}^{-1}(\boldsymbol{D}_{\mathrm{ll}} + \boldsymbol{D}_{\mathrm{rr}}) \end{pmatrix} \begin{pmatrix} \boldsymbol{p}_{\mathrm{l}} \\ \lambda \boldsymbol{p}_{\mathrm{l}} \end{pmatrix} = \lambda \begin{pmatrix} \boldsymbol{p}_{\mathrm{l}} \\ \lambda \boldsymbol{p}_{\mathrm{l}} \end{pmatrix} \tag{7}$$

The velocity component can then be obtained by:

$$\boldsymbol{v}_{\mathrm{l}} = (\boldsymbol{D}_{\mathrm{ll}} + \lambda \boldsymbol{D}_{\mathrm{lr}})\boldsymbol{p}_{\mathrm{l}} \tag{8}$$

Each eigenvector $\boldsymbol{\phi}_j$ can be divided into pressure and velocity components:

$$\boldsymbol{\phi}_j = \begin{Bmatrix} \boldsymbol{\phi}_{\mathbf{p}} \\ \boldsymbol{\phi}_{\mathbf{v}} \end{Bmatrix}_j \tag{9}$$

The matrix of the eigenvectors $\boldsymbol{\phi}$ can be then written as follows:

$$\boldsymbol{\phi} = \begin{pmatrix} \boldsymbol{\phi}_{\mathbf{p}}^{\mathrm{inc}} & \boldsymbol{\phi}_{\mathbf{p}}^{\mathrm{ref}} \\ \boldsymbol{\phi}_{\mathbf{v}}^{\mathrm{inc}} & \boldsymbol{\phi}_{\mathbf{v}}^{\mathrm{ref}} \end{pmatrix} \tag{10}$$

The eigenvectors refer to the wave modes, while the eigenvalues yield the axial wavenumbers as in Eq. (11):

$$k_j = -\frac{\ln(\lambda_j)}{\mathrm{i}\Delta} \tag{11}$$

i is the complex number verifying $\mathrm{i}^2 = -1$. The pressures and velocities are given by:

$$\boldsymbol{p} = \boldsymbol{\phi}_{\mathbf{p}}^{\mathrm{inc}}\boldsymbol{Q}^{\mathrm{inc}} + \boldsymbol{\phi}_{\mathbf{p}}^{\mathrm{ref}}\boldsymbol{Q}^{\mathrm{ref}} \tag{12}$$

$$\boldsymbol{v} = \boldsymbol{\phi}_{\mathbf{v}}^{\mathrm{inc}}\boldsymbol{Q}^{\mathrm{inc}} + \boldsymbol{\phi}_{\mathbf{v}}^{\mathrm{ref}}\boldsymbol{Q}^{\mathrm{ref}} \tag{13}$$

with $\boldsymbol{Q}^{\mathrm{t}} = [(\boldsymbol{Q}^{\mathrm{inc}})^{\mathrm{t}}(\boldsymbol{Q}^{\mathrm{ref}})^{\mathrm{t}}]$ are the modal amplitudes where t stands for the transpose.

Let us consider now a waveguide submitted to a pressure and an acoustic impedance at its left and right ends, respectively. The waveguide is divided into N segments. Boundary conditions are therefore expressed as follows:

$$\boldsymbol{\phi}_{\mathbf{p}}^{\text{inc}}\,\mathbf{Q}^{\,\text{inc}(1)} + \boldsymbol{\phi}_{\mathbf{p}}^{\text{ref}}\,\mathbf{Q}^{\,\text{ref}(1)} = \boldsymbol{p}_0 \tag{14}$$

$$\boldsymbol{\Lambda}^{-N}\,\mathbf{Q}^{\,\text{ref}(1)} = \boldsymbol{R}\boldsymbol{\Lambda}^{N}\,\mathbf{Q}^{\,\text{inc}(1)} \tag{15}$$

Superscript (i) refers to the ith cross-sectional surface of the waveguide, $\boldsymbol{p}_0$ is the magnitude of the imposed pressure, N is the number of cells composing the duct, $\boldsymbol{\Lambda}$ is the $n_{\text{d}} \times n_{\text{d}}$ diagonal matrix of eigenvalues λ_j^{inc} corresponding to the incident modes, and $\boldsymbol{R}$ stands for a diagonal reflection matrix.

The system is solved for $(\mathbf{Q}^{\,\text{inc}(1)}, \mathbf{Q}^{\,\text{ref}(1)})$, and a subsequent application of the Bloch theorem provides the amplitudes anywhere inside the waveguide. It is clear that the CPU time depends on the matrix sizes, that is to say that the sectional mesh density only. However, direct inversion of the systems (14) and (15) is prone to numerical issues. The resolution will benefit from a mathematical manipulation leading to:

$$\begin{pmatrix} \mathbf{Q}^{\,\text{inc}(1)} \\ \mathbf{Q}^{\,\text{ref}(1)} \end{pmatrix} = \begin{pmatrix} \boldsymbol{I}_{n_{\text{d}}} & \mathbf{0} \\ \mathbf{0} & \boldsymbol{\Lambda}^{N} \end{pmatrix} \begin{pmatrix} \boldsymbol{I}_{n_{\text{d}}} & (\boldsymbol{\phi}_{\mathbf{p}}^{\text{inc}})^{-1}(\boldsymbol{\phi}_{\mathbf{p}}^{\text{ref}})\boldsymbol{\Lambda}^{N} \\ \boldsymbol{R}\boldsymbol{\Lambda}^{N} & -\boldsymbol{I}_{n_{\text{d}}} \end{pmatrix}^{-1} \begin{pmatrix} (\boldsymbol{\phi}_{\mathbf{p}}^{\text{inc}})^{-1}\boldsymbol{p}_0 \\ \mathbf{0} \end{pmatrix} \tag{16}$$

The pressure vector for the ith cross section is given by:

$$\boldsymbol{p}^{(i)} = \begin{pmatrix} \boldsymbol{\phi}_{\mathbf{p}}^{\text{inc}} & \boldsymbol{\phi}_{\mathbf{p}}^{\text{ref}} \end{pmatrix} \begin{pmatrix} \boldsymbol{\Lambda}^{i-1} & \mathbf{0} \\ \mathbf{0} & \boldsymbol{\Lambda}^{-(i-1)} \end{pmatrix} \begin{pmatrix} \mathbf{Q}^{\,\text{inc}(1)} \\ \mathbf{Q}^{\,\text{ref}(1)} \end{pmatrix} \tag{17}$$

It should be noted that, when i becomes large, numerical difficulties may arise when calculating the forced response. This is because $\boldsymbol{\Lambda}^{-(i-1)}$ in Eq (17) tends to infinity in this case. A solution for this issue is to retain only the propagating and the less decaying waves and eliminate the strongly evanescent waves for which $|\lambda| < \delta$, where δ is a user-defined value [27,15]. The waves for which $|\lambda|$ is too small are rapidly decaying and almost with no contribution to the overall response while they do cause numerical issues.

2.2. Scattering matrix

The scattering matrix is a characterisation of a lined part of the duct without regard to the upstream and downstream acoustic conditions. Indeed, it depends only on geometric and acoustic characteristics of the duct, and relates the outgoing pressure amplitudes $\boldsymbol{P}_{\text{out}}$ to the incoming pressure amplitudes $\boldsymbol{P}_{\text{in}}$ as follows:

$$\boldsymbol{P}_{\text{out}} = \boldsymbol{C}\,\boldsymbol{P}_{\text{in}} \tag{18}$$

The scattering matrix $\boldsymbol{C}$ was computed through the WFE method as was done in [9]. The condensed dynamic stiffness matrix $\boldsymbol{D}_{\mathbf{c}}$ of the lined part must be first calculated. The scattering matrix is then given by:

$$\boldsymbol{C} = -\left(\boldsymbol{D}_{\mathbf{c}}\boldsymbol{\psi}_{\mathbf{p}}^{\text{ref}} + \boldsymbol{\psi}_{\mathbf{v}}^{\text{ref}}\right)^{+}\left(\boldsymbol{D}_{\mathbf{c}}\boldsymbol{\psi}_{\mathbf{p}}^{\text{inc}} + \boldsymbol{\psi}_{\mathbf{v}}^{\text{inc}}\right) \tag{19}$$

where

$$\boldsymbol{\psi}_{\mathbf{p}}^{\text{inc}} = \begin{pmatrix} \boldsymbol{\phi}_{\mathbf{p}}^{\text{inc}} & \mathbf{0} \\ \mathbf{0} & \boldsymbol{\phi}_{\mathbf{p}}^{\text{ref}} \end{pmatrix} \quad \boldsymbol{\psi}_{\mathbf{p}}^{\text{ref}} = \begin{pmatrix} \boldsymbol{\phi}_{\mathbf{p}}^{\text{ref}} & \mathbf{0} \\ \mathbf{0} & \boldsymbol{\phi}_{\mathbf{p}}^{\text{inc}} \end{pmatrix}$$

$$\boldsymbol{\psi}_{\mathbf{v}}^{\text{inc}} = \begin{pmatrix} \boldsymbol{\phi}_{\mathbf{v}}^{\text{inc}} & \mathbf{0} \\ \mathbf{0} & -\boldsymbol{\phi}_{\mathbf{v}}^{\text{ref}} \end{pmatrix} \quad \boldsymbol{\psi}_{\mathbf{v}}^{\text{ref}} = \begin{pmatrix} \boldsymbol{\phi}_{\mathbf{v}}^{\text{ref}} & \mathbf{0} \\ \mathbf{0} & -\boldsymbol{\phi}_{\mathbf{v}}^{\text{inc}} \end{pmatrix}$$

and $^{+}$ stands for the pseudo inverse. The pseudo inverse is used rather than the inverse to avoid errors due to ill-conditioned matrices inversion. With an arrangement of the modal amplitudes leading to the above-presented expression, reflection coefficients correspond to terms of the diagonal square blocks of the scattering matrix $\boldsymbol{C}$, while transmission coefficients correspond to terms of the off-diagonal square blocks.

2.3. Acoustic impedance of a perforated plate backed by a cavity

Several empirical models used to calculate the perforated plates impedance have been developed in previous works [24, 26]. Resistance r and reactance χ have been given in terms of medium properties and geometric parameters of the material (Table 1).

When the acoustic velocity and the flow effects are not taken into account, the Guess linear model, detailed in [24], is given as follows.

For $ke << 1$, $kd/2 < 1/4$ and $|k_s d/2| > 10$:

$$r = \frac{\sqrt{8\nu\omega}}{\varphi c}\left(1 + \frac{e}{d}\right) + \frac{1}{8\varphi}(kd)^2 \tag{20}$$

Table 1
Signification of the different parameters.

Medium properties	Geometric parameters
k: wavenumber	e: plate thickness
f: frequency; ω: angular frequency	d: orifice diameter
ν: kinematic viscosity of the fluid	φ: porosity
c: sound celerity; ρ: density	
$k_s = (i\omega/\nu)^{1/2}$: Stokes wavenumber	

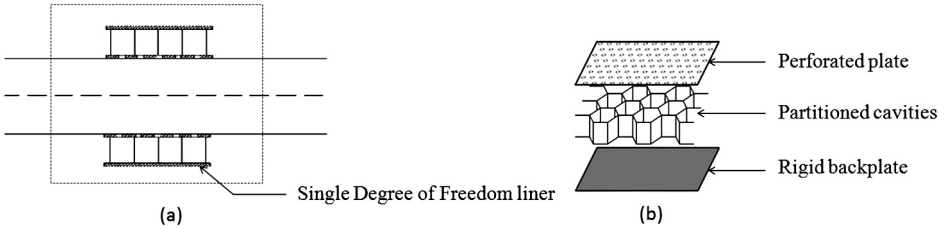

Fig. 2. Calculation domain (a) and composition of the liner (b).

$$\chi = \frac{\omega}{\varphi c}\left[e + \frac{8d}{3\pi}(1 - 0.7\sqrt{\varphi}) + \sqrt{\frac{8\nu}{\omega}}(1 + \frac{e}{d})\right] \tag{21}$$

r and χ are respectively the resistance and the reactance of the perforated plate. The empirical term $(1 - 0.7\sqrt{\varphi})$ is used as a correction instead of the Fok function to express the hole interaction effect.

A schematic of a locally reacting liner is represented in Fig. 2. The treatment is composed of a perforated plate, a honeycomb structure, and a rigid backplate. The sectional area dimensions of the cavities must be small compared to the minimal wave length. This is in fact the main hypothesis that makes the liner considered a locally reacting one: Waves will only travel in the direction normal to the perforated plate inside cavities. The expression of the impedance in this case is independent of the direction of the incident waves, and depends only on the frequency, the geometry, and the properties of the fluid.

Therefore, the normalised impedance of a perforated plate backed by a cavity Z is given by adding the cavity impedance to the perforated plate impedance:

$$Z = r + \mathrm{i}(\chi - \cot(kD)) \tag{22}$$

where D is the depth of the cavity.

2.4. Equivalent fluid model of porous materials

Assuming that the frame is rigid, a porous material can be defined using the Johnson–Champoux–Allard equivalent fluid model. The wave equation is written as follows [28]:

$$\nabla^2 p + \omega^2 \frac{\tilde{\rho}}{\tilde{K}} p = 0 \tag{23}$$

where $\tilde{\rho}$ and $\tilde{K}$ are respectively the effective density and effective bulk modulus and are given as:

$$\tilde{\rho}(\omega) = \frac{\sigma\varphi}{\mathrm{i}\omega}\left[1 + \frac{4\mathrm{i}\alpha_\infty^2 \eta\omega\rho}{\varphi^2\Lambda^2\sigma^2}\right]^{1/2} + \rho\alpha_\infty \tag{24}$$

and

$$\tilde{K}(\omega) = \frac{P_0\gamma}{\gamma - (\gamma - 1)\left[\dfrac{8\eta}{\mathrm{i}\omega\rho Pr\Lambda'^2}\left(1 + \dfrac{\Lambda'^2\mathrm{i}\omega\rho Pr}{16\eta}\right)^{1/2} + 1\right]^{-1}} \tag{25}$$

where σ is the fluid resistivity, φ is the porosity, α_∞ is the tortuosity, η is the dynamic viscosity, ρ is the density of the fluid, Λ is the viscous characteristic length, Λ' is the thermal characteristic length, P_0 is the static reference pressure, γ is the ratio of specific heats at respectively constant pressures and volumes defined as $\gamma = C_p/C_v$, and Pr is the Prandtl number.

It is worth noting that $\tilde{\rho}$ and $\tilde{K}$ are complex and frequency dependent. The complex wavenumber in the equivalent fluid model k_e is expressed as follows:

$$k_e = \frac{\omega}{c_e} = \omega\sqrt{\frac{\tilde{\rho}}{\tilde{K}}} \tag{26}$$

where c_e is the sound celerity in the equivalent fluid. Further, the mass and stiffness elementary matrices $\boldsymbol{M}^e$ and $\boldsymbol{K}^e$ are respectively given by:

$$\boldsymbol{M}^e = \iiint_{\Omega} \frac{1}{\tilde{\rho}c_e^2}\boldsymbol{N}\boldsymbol{N}^t \mathrm{d}v \tag{27}$$

$$\boldsymbol{K}^e = \iiint_{\Omega} \frac{1}{\tilde{\rho}}[\nabla \boldsymbol{N}]^t[\nabla \boldsymbol{N}]\,\mathrm{d}v \tag{28}$$

where $\boldsymbol{N}$ is the column vector of shape functions N_i, $[\nabla \boldsymbol{N}]$ is the matrix of vectors ∇N_i, t stands for the transpose and Ω is the volume domain of a single element.

The surface impedance $Z_s(\theta)$ of the equivalent fluid is given as follows [29]:

$$Z_s(\theta) = -\mathrm{i}Z_c\frac{k_e}{k_{e,n}}\cot(k_{e,n}d_e) \tag{29}$$

where Z_c is the characteristic impedance of the equivalent fluid, d_e is the thickness of the equivalent fluid layer, and $k_{e,n}$ is the component of wavenumber k_e in the direction normal to the walls is given by:

$$k_{e,n} = \sqrt{k_e^2 - \left(\frac{\omega}{c}\sin\theta\right)^2} \tag{30}$$

with θ is the incidence angle of the mode and is expressed as follows:

$$\theta = \arccos\left(\sqrt{1 - \left(\frac{f^c}{f}\right)^2}\right) \tag{31}$$

f^c is the cut-off frequency of the mode. The reflection coefficient from the porous layer to the medium is further given by:

$$R = \frac{Z_s\cos\theta - \rho c}{Z_s\cos\theta + \rho c} \tag{32}$$

2.5. Acoustic power attenuation and transmission loss

The acoustic power attenuation W_{att} can be calculated from the scattering matrix as described below [30]:

$$W_{att} = 10\log\left(\frac{W_{in}}{W_{out}}\right) \tag{33}$$

W_{in} refers to as the incident acoustic power, and is given in this case as follows:

$$W_{in} = \boldsymbol{P}^h\boldsymbol{Y}\boldsymbol{P} \tag{34}$$

where $\boldsymbol{P} = \left\langle \ldots P_{mn}^{(1)+} \ldots, \ldots P_{mn}^{(2)-} \ldots \right\rangle^t$ is the vector of modal pressures incident to the left and right duct sections where m stands for the circumferential mode order and n is the radial mode order, h denotes the conjugate transpose and $\boldsymbol{Y}$ is the diagonal matrix defined such as:

$$\boldsymbol{Y} = \begin{pmatrix} \boldsymbol{Y}_{11} & \boldsymbol{0} \\ \boldsymbol{0} & \boldsymbol{Y}_{22} \end{pmatrix} \tag{35}$$

with $\boldsymbol{Y}_{11}$ and $\boldsymbol{Y}_{22}$ are the diagonal matrices with $(N_{mn}k_{mn})/(2\rho\omega)$ on the diagonals. N_{mn} are the coefficients associated with the (m, n) mode defined for a cylindrical duct as:

$$N_{mn} = \pi a^2 J_m^2(\chi_{mn})\left(1 - \frac{m^2}{\chi_{mn}^2}\right) \tag{36}$$

and $N_{00} = 1$, where a is the radius of the duct, J_m is the Bessel function of the first kind of order m and χ_{mn} is the nth root satisfying the hard-wall boundary condition: $J'_m(\chi_{mn}) = 0$.

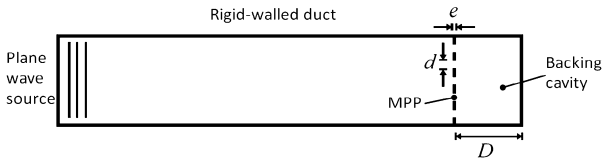

Fig. 3. Rigid cylindrical duct ended by a perforated plate and a backing cavity.

W_{out} corresponds to the outgoing pressures from the left and right duct sections. In the present work, the incident modes are assumed to have random initial phases. In this case, W_{out} is given as follows [21]:

$$W_{\text{out}} = \boldsymbol{P}^h \,\text{diag}(\boldsymbol{C}^h \boldsymbol{Y} \boldsymbol{C})\, \boldsymbol{P} \tag{37}$$

$\boldsymbol{C}$ is the scattering matrix defined in Eq. (19).

When calculating the transmission loss, the expression of the incident acoustic power $W_{\text{in}}^{(1)}$ becomes:

$$W_{\text{in}}^{(1)} = \boldsymbol{P}_1^h \boldsymbol{Y}_{11} \boldsymbol{P}_1 \tag{38}$$

with $\boldsymbol{P}_1 = \left\langle \ldots P_{mn}^{(1)+} \ldots \right\rangle^{\text{t}}$ is the vector of modal pressures incident to the left duct section. Taken into consideration the random phases assumption, the transmitted acoustic power $W_{\text{out}}^{(2)}$ is given by [21]:

$$W_{\text{out}}^{(2)} = \boldsymbol{P}_1^h \,\text{diag}(\boldsymbol{T}^h \boldsymbol{Y}_{11} \boldsymbol{T})\, \boldsymbol{P}_1 \tag{39}$$

Here, $\boldsymbol{T}$ stands for the transmission matrix. The transmission loss TL is finally given by:

$$TL = 10 \log \left(\frac{W_{\text{in}}^{(1)}}{W_{\text{out}}^{(2)}} \right) \tag{40}$$

3. Numerical examples

3.1. Sound propagation in ducts with locally reacting lining

Two different cases are considered. The first one deals with the forced response of a rigid duct with a termination treatment. The second one is devoted to the calculation of the scattering matrix for ducts composed of two hard-walled parts and a part with a locally reacting liner in between. Here, the equivalent surface impedance is calculated for both cases.

3.1.1. Forced response of a rigid duct with perforated plate and backing cavity termination

This section deals with the prediction of the sound pressure in a hard-walled duct. The studied medium is supposed to be periodic with a plane-wave mode excitation at inlet and a perforated plate backed by a cavity at outlet as shown in Fig. 3. In this case, the WFE approach is used and compared to the conventional Finite Element method using ANSYS [31].

In order to study the frequency response of the medium using ANSYS, the duct was discretised using the FLUID30 elements in a harmonic analysis. To introduce the termination impedance, the surface effect element SURF154 was used. Since these are structural elements, every single fluid element in contact with the SURF154 elements must have the displacement degrees of freedom activated. The fluid–structure interaction flag is applied. All other FLUID30 elements have only the pressure degree of freedom. The resistance is defined as the viscosity of the material. As the impedance is a function of the frequency and the reactance is less than zero for the low frequencies and greater than zero for the high frequencies, one of two ways has to be adopted for introducing the reactance, depending on the sign of the imaginary part of the impedance. For the frequency range where the reactance is positive, the additional mass per unit area is used. Elsewhere, the elastic foundation stiffness is used. It is not possible to tabulate the real element constants. So, an iteration along with the solve command is issued switching between the mass or stiffness definitions following the sign of the imaginary impedance [31]. The magnitudes of the pressure excitation are equal to 1 Pa. Since pressures are applied equally to the nodes, the plane-wave mode was generated. The radius of the duct is 0.04 m. The length of the duct is $L = 0.24$ m. The length of the segments composing the duct used for the WFE method is 0.002 m. The depth of the cavity is $D = 0.01$ m. In this example, a porosity $\varphi = 1\%$, a plate thickness $e = 0.001$ m, and a diameter of the orifices $d = 0.001$ m is considered. 19360 fluid elements were used for the FE model.

The axial wavenumbers can be calculated using the WFE method by means of Eq. (11). Fig. 4 represents the evolution of the real parts of the axial wavenumbers corresponding to the forward-going waves in the frequency range 0 Hz–7000 Hz, validated by analytical solutions. The figure shows a good agreement between the two approaches. The evolution of the normalised impedance at the end of the duct is shown in Fig. 5. The frequency evolution of the pressure magnitude at $z = L/2$ is represented in Fig. 6. The continuous curve represents the frequency response using the proposed approach. The dotted curve represents the validation by the full FE model.

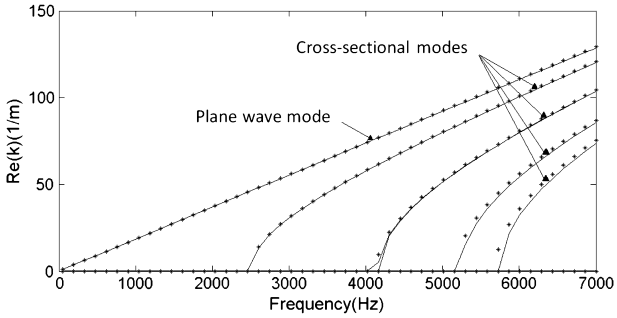

Fig. 4. Frequency evolution of the axial wavenumber real parts corresponding to the forward-going waves for an 8-cm-diameter waveguide: (–) WFE method; (∗) analytical solutions.

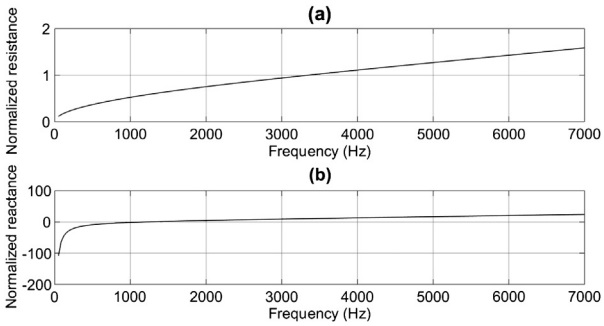

Fig. 5. Normalised resistance (a) and normalised reactance (b) at the end of the duct computed using the linear Guess model.

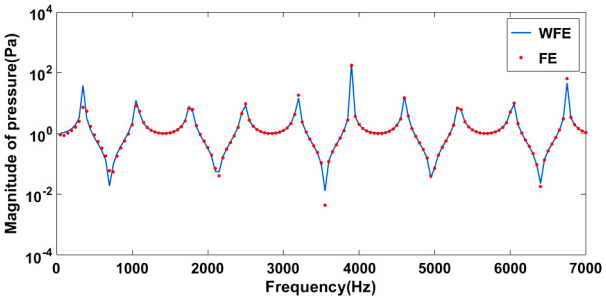

Fig. 6. Frequency evolution of the pressure magnitude at $z = L/2$ within a rigid duct submitted to the mode $(0, 0)$ and ended by a perforated plate and a backing cavity.

Table 2
FE and WFE computing times for a 1-m-long duct and for the same machine capacities.

Method	CPU time	CPU time reduction percentage
FEM	457.02 s	–
WFEM	65.11 s	85,75%

To illustrate the CPU time reduction by the WFE method compared to the conventional FE method, the elapsed times for the calculation of the forced response of a 1-m-long duct are represented in Table 2.

3.1.2. Scattering coefficients for lined ducts

This section deals with the evaluation of the scattering coefficients for periodic ducts with impedance discontinuity. We consider a cylindrical duct (see Fig. 7). The study was performed at up to 8000 Hz for a diameter of 0.16 m, and a lined length of 0.015 m. Twenty-four modes are cut-on at the maximal frequency, and at the highest frequency at which only the plane-wave mode propagates is ≈1245 Hz.

The wave characteristics of the rigid parts of the duct were first evaluated using the WFE approach. Some mode shapes of the rigid waveguide parts are represented in Table 3 through the use of the WFE method and the conventional FE approach.

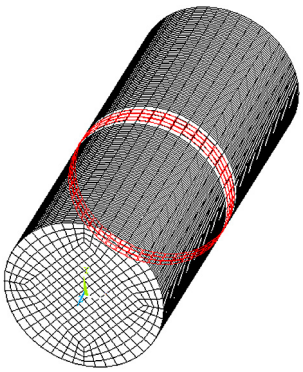

Fig. 7. Finite Element model of the cylindrical duct with a lined part.

Table 3
Modes shapes.

Mode	WFE simulation	FE simulation
(0, 0)	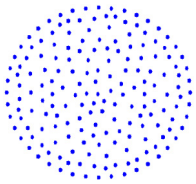	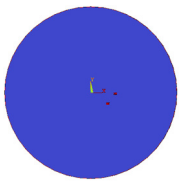
(1, 0)	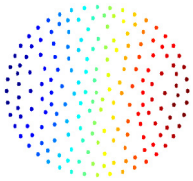	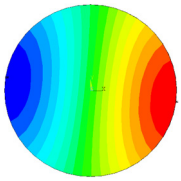
(0, 1)	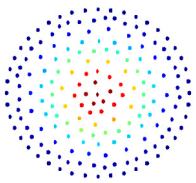	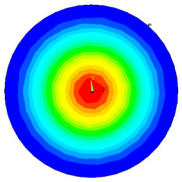
(1, 1)	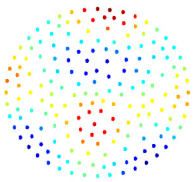	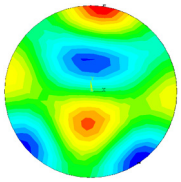
(5, 0)	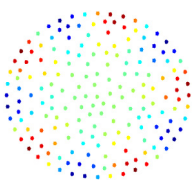	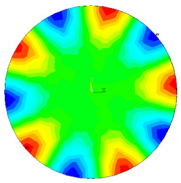

The lined part represents the discontinuity within the duct. We consider: porosity $\varphi = 3$. The scattering matrix was also computed for validation using the analytical method as was detailed in [20] with a sufficient number of truncated modes.

The frequency evolution of the scattering coefficients can be then represented for different modes (m, n) by both methods, where m and n stand for the circumferential and radial mode orders, respectively. Letters 'T' and 'R' denote transmission and reflection, respectively. Only transmission from one of the two sides to the other side and reflection from the lined part to one of the two sides were studied, as the problem is symmetric.

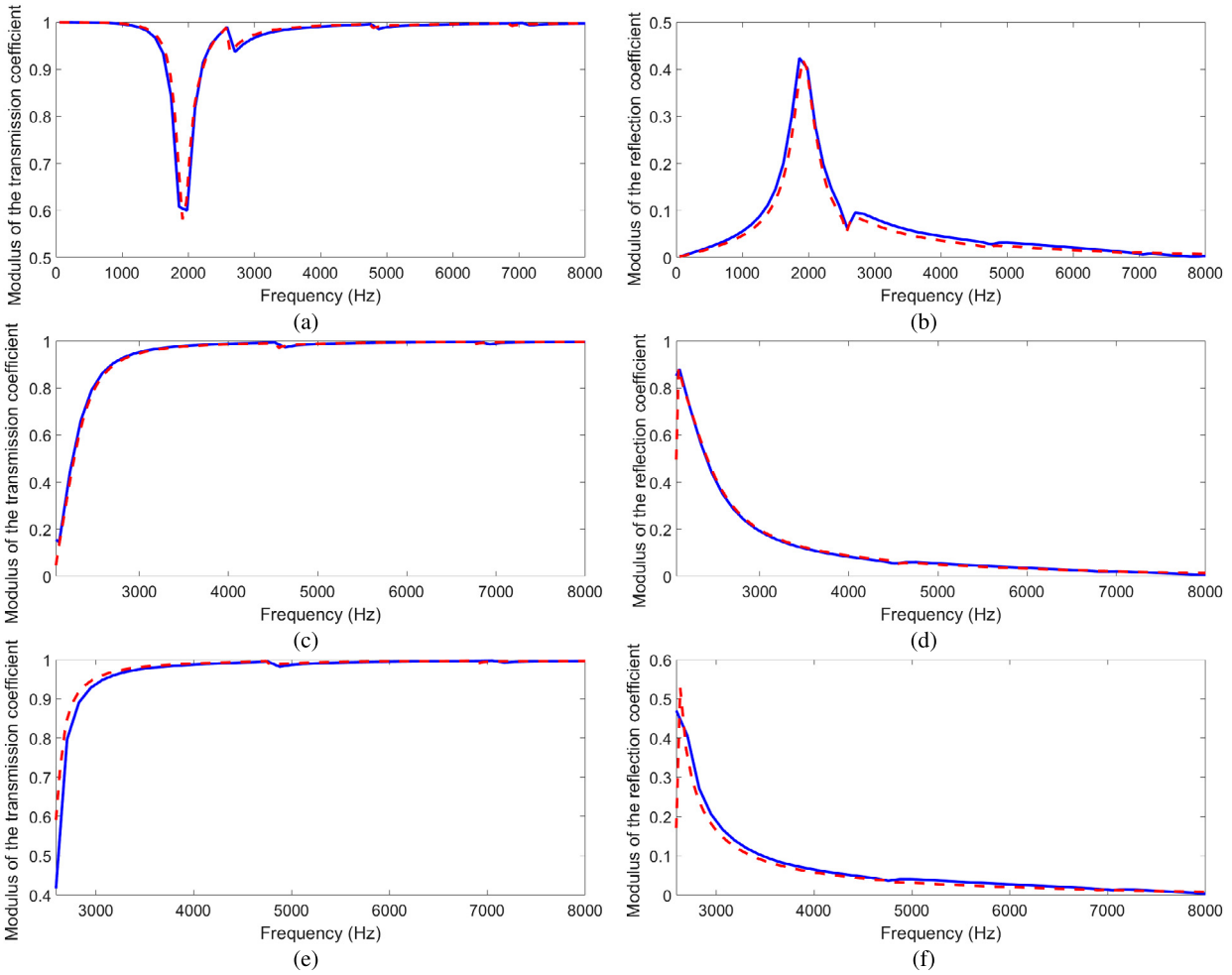

Fig. 8. Frequency evolution of the transmission coefficients: (a) T((0, 0), (0, 0)), (c) T((2, 0), (2, 0)), (e) T((0, 1), (0, 1)) and reflection coefficients, (b) R((0, 0), (0, 0)), (d) R((2, 0), (2, 0)), (f) R((0, 1), (0, 1)) (—). WFE method (- - -). Analytical method.

Each incident mode reflects and transmits into a modal spectrum. Figs. 8(a) and 8(b) show, respectively, the transmission and reflection coefficients moduli of the plane-wave mode. The scattering of higher orders modes was moreover studied. Figs. 8(c) and 8(d) show respectively the transmission and reflection coefficients moduli of mode (2, 0). Transmission and reflection coefficients moduli of the mode (0, 1) are represented in Figs. 8(e) and 8(f), respectively.

Because of the circumferential symmetry of the duct, there is no scattering from a mode into another mode with a different m order. Therefore, only modes with same circumferential order exchange energy. The conversion coefficients correspond to the off-diagonal terms of the transmission and reflection matrices. Figs. 9(a) and 9(b) represent the conversion of the plane-wave mode with mode (0, 1). The conversion of the modes (2, 0) and (2, 1) is shown in Figs. 9(c) and 9(d).

The figures show a fair agreement between the WFE method and the analytical method. It is also noted from Fig. 9 that conversion between the m-modes exists and is maximal for the frequencies at which they become cut-on. This result matches well the slight changes in the shapes of the curves in Figs. 8(a), 8(b), 8(c) and 8(d) near the cut-off frequencies of the higher-order modes.

It is also shown from the previous results that the scattering coefficients for liners made of honeycombs depend highly on frequency. Maximal reflection is reached when the impedance is purely resistive. Honeycombs are designed to absorb sound in a particular frequency range. Therefore, the variation of the geometric parameters affects the liner performances.

3.1.3. Effect of the geometric parameters on the liner efficiency

The liner efficiency can be evaluated through the calculation of the acoustic power attenuation and transmission loss. In this section, the effect of the geometric parameters on the liner efficiency is studied by varying one of the parameters at a time and leaving the others unchanged. The effects of the porosity and the thickness of the perforated plate and of the diameter of the holes are investigated. Figs. 10, 11 and 12 show the effect of porosity, plate thickness and hole diameter on

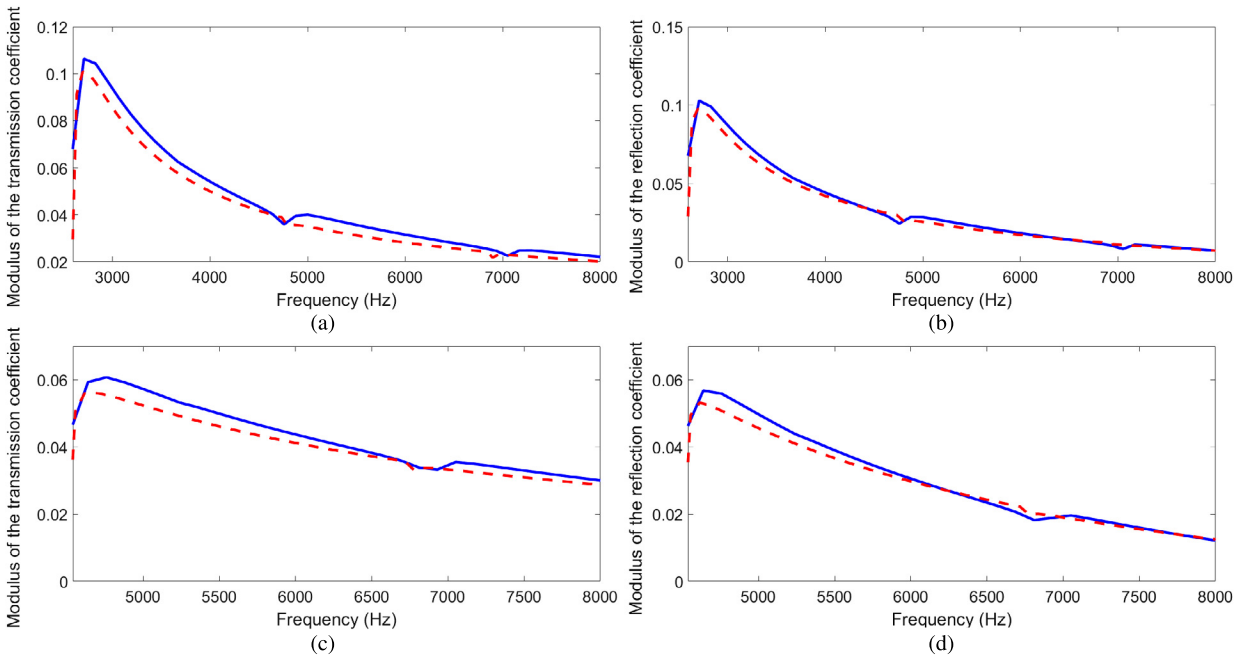

Fig. 9. Frequency evolution of the transmission coefficients: (a) T((0, 0), (0, 1)), (c) T((2, 0), (2, 1)) and reflection coefficients (b) R((0, 0), (0, 1)), (d) R((2, 0), (2, 1)). (–) WFE method (- - -). Analytical method.

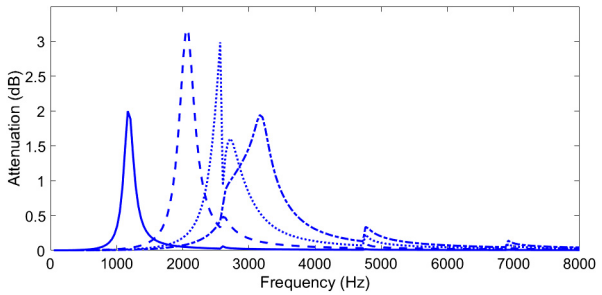

Fig. 10. Effect of the porosity φ of the perforated plate on the acoustic power attenuation of the lined duct part: (–) $\varphi = 1\%$; (- -) $\varphi = 3\%$; (. . .) $\varphi = 5\%$; (- . -) $\varphi = 7\%$.

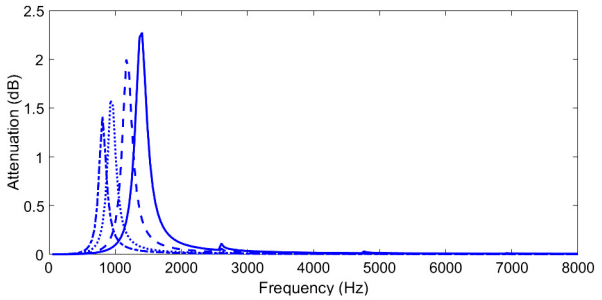

Fig. 11. Effect of the thickness e of the perforated plate on the acoustic power attenuation of the lined duct part: (–) $e = 0.5{\cdot}10^{-3}$ m; (- -) $e = 1{\cdot}10^{-3}$ m; (. . .) $e = 2{\cdot}10^{-3}$ m; (- . -) $e = 3{\cdot}10^{-3}$ m.

acoustic power attenuation, respectively. Figs. 13, 14 and 15 show the effect of porosity, plate thickness and hole diameter on the transmission loss, respectively.

It has been already shown that the frequency of maximal attenuation depends on the geometric parameters of the liner. The attenuation is maximal when the liner's impedance is purely resistive. Furthermore, as expected, it is noted that

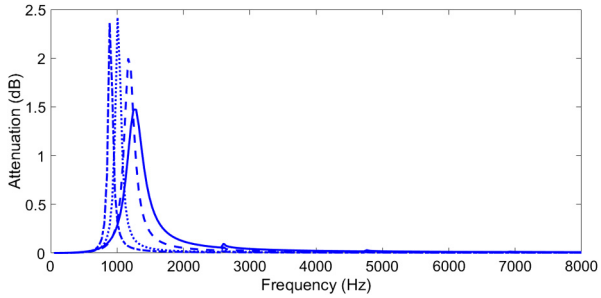

Fig. 12. Effect of the diameter d of the orifices of the perforated plate on the acoustic power attenuation of the lined duct part: (–) $d = 0.5{\cdot}10^{-3}$ m; (- -) $d = 1{\cdot}10^{-3}$ m; (. . .) $d = 2{\cdot}10^{-3}$ m; (- . -) $d = 3{\cdot}10^{-3}$ m.

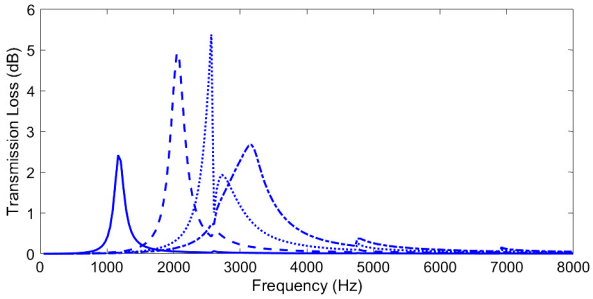

Fig. 13. Effect of the porosity φ of the perforated plate on the transmission loss of the lined duct part: (–) $\varphi = 1\%$; (- -) $\varphi = 3\%$; (. . .) $\varphi = 5\%$; (- . -) $\varphi = 7\%$.

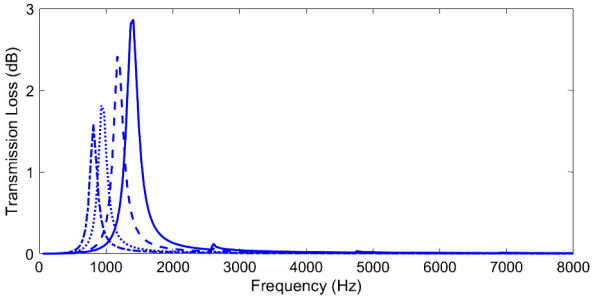

Fig. 14. Effect of the thickness e of the perforated plate on the transmission loss of the lined duct part: (–) $e = 0.5{\cdot}10^{-3}$ m; (- -) $e = 1{\cdot}10^{-3}$ m; (. . .) $e = 2{\cdot}10^{-3}$ m; (- . -) $e = 3{\cdot}10^{-3}$ m.

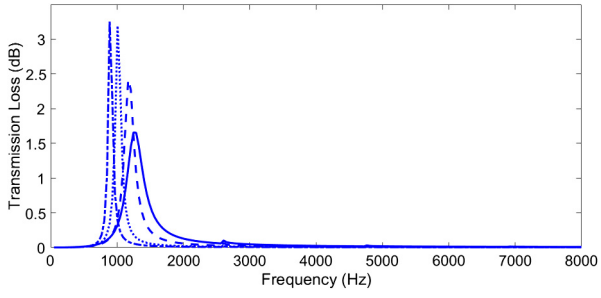

Fig. 15. Effect of the diameter d of orifices of the perforated plate on the transmission loss of the lined duct part: (–) $d = 0.5{\cdot}10^{-3}$ m; (- -) $d = 1{\cdot}10^{-3}$ m; (. . .) $d = 2{\cdot}10^{-3}$ m; (- . -) $d = 3{\cdot}10^{-3}$ m.

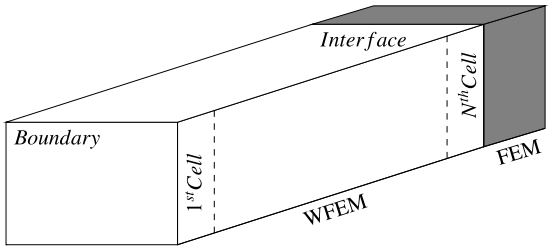

Fig. 16. Description of the boundary conditions problem.

transmission losses are greater than attenuations. This is a predictable consequence as the transmission loss of the acoustic power includes reflection as well as absorption, contrarily to attenuation, which only characterises absorption by the liner.

3.2. Sound propagation in ducts with porous lining

3.2.1. Forced response of rigid ducts with a porous layer termination

In the current section, the response of guided waves incident to porous interfaces is explored. Let us consider a rigid duct ended by a porous material layer. The porous material layer is backed by a rigid wall. The pressure amplitudes were first computed by the WFE method. Two alternatives are here used:

(1) replacing the porous layer by an equivalent acoustic impedance as in Eq. (29). The reflection is calculated, and therefore a reflection condition is defined as a boundary condition at the end of the duct;

(2) three-dimensional modelling of the porous domain, i.e. the solution provided by the full FE model of the lining using Eqs. (27) and (28) (see Fig. 16 and Appendix A). The boundary conditions are expressed as follows:

$$\boldsymbol{\phi}_{\mathbf{p}}^{\text{inc}}\,\mathbf{Q}^{\,\text{inc}(1)} + \boldsymbol{\phi}_{\mathbf{p}}^{\text{ref}}\,\mathbf{Q}^{\,\text{ref}(1)} = \boldsymbol{p}_0 \tag{41}$$

$$\begin{pmatrix} \boldsymbol{\phi}_{\mathbf{p}}^{\text{inc}}\,\mathbf{Q}^{\,\text{inc}(N+1)} + \boldsymbol{\phi}_{\mathbf{p}}^{\text{ref}}\,\mathbf{Q}^{\,\text{ref}(N+1)} \\ \boldsymbol{\phi}_{\mathbf{v}}^{\text{inc}}\,\mathbf{Q}^{\,\text{inc}(N+1)} + \boldsymbol{\phi}_{\mathbf{v}}^{\text{ref}}\,\mathbf{Q}^{\,\text{ref}(N+1)} \end{pmatrix} = \begin{pmatrix} \boldsymbol{p}_l \\ -\boldsymbol{v}_l \end{pmatrix} \tag{42}$$

where superscript (i) refers to the ith cross section of the rigid duct part, subscripts $\mathbf{p}$ and $\mathbf{v}$ refer respectively to the pressure and velocity block components of the matrix of eigenvectors calculated by the WFE eigenproblem, N is the number of segments composing the air-filled waveguide, $\boldsymbol{p}_{\text{l}}$ and $\boldsymbol{v}_{\text{l}}$ are pressures and velocities vectors corresponding to the left surface of the equivalent fluid.

The porous domain was discretised using cubic elements and linear interpolation functions. The differentials of the shape functions with respect to x, y and z are expressed using differentials with respect to the natural coordinates, and elementary mass and stiffness matrices of the equivalent fluid are calculated. The matrices are finally assembled.

The WFE results were then compared to the FE solution using the harmonic analysis carried out by ANSYS. The Johnson–Champoux–Allard model is activated for the porous material and the physical constants are used as input. It is worth noting that the implementation in the ANSYS 14.5 release uses the effective terms as defined in Eqs. (24) and (25), and is not what a user would expect, as one should normally solve for the equivalent terms (divided by porosity) [31].

A hard-walled duct with a 0.056 m $\times$ 0.04 m rectangular cross section was considered. The thickness of the porous layer is 0.01 m. The properties of the porous material are: $\sigma = 1000\ \text{N s/m}^4$, $\varphi = 0.88$, $\alpha_\infty = 1$, $\Lambda = 129{\cdot}10^{-6}$ m, and $\Lambda' = 198{\cdot}10^{-6}$ m. Figs. 17 and 18 show the frequency evolution of the pressure amplitude in one point inside the duct submitted to the $(0,0)$ and $(1,1)$ modes, respectively. For the case of the excitation by the mode $(1,1)$, the forced response was presented from 5000 Hz, since the wave is evanescent for the lower frequencies.

3.2.2. Acoustic scattering of a hard-walled porous domain transition in ducts

In this section, the scattering from a porous layer inside a duct is studied. Let us consider the waveguide presented in Fig. 19. The porous medium is defined using the Johnson–Champoux–Allard model. The elementary mass and stiffness matrices are assembled to obtain the matrices of the porous part. The dynamic stiffness matrix of the porous domain is calculated and condensed onto its left and right ends. Then, the scattering matrix is expressed as in Eq. (19). The forced response is first calculated through the equations provided by the WFE method [23]. The results are then compared to the full FE analysis by ANSYS.

Dimensions of the cross section of the above-mentioned waveguide are 0.056 m $\times$ 0.04 m. The depth of the porous layer is 0.015 m. The same constants as those considered in the previous section were used for the porous material modeling. Figs. 20 and 21 show the pressure magnitudes for a duct submitted to the pressure mode $(0,0)$ at both ends, and a duct submitted to the pressure mode $(0,0)$ and ended by rigid wall, respectively.

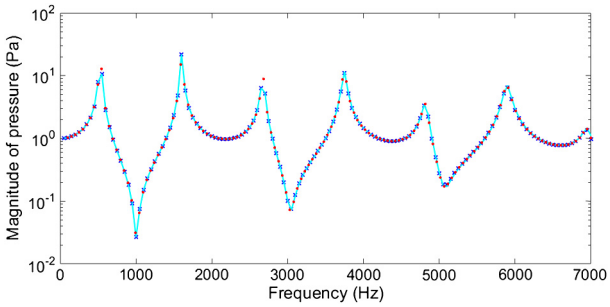

Fig. 17. Frequency evolution of the pressure magnitude in one point within a rigid duct submitted to the mode $(0, 0)$ and ended by a porous layer: $(\times)$ WFE method + equivalent impedance; $(-)$ WFE method + FE boundary; $(.)$ FE method.

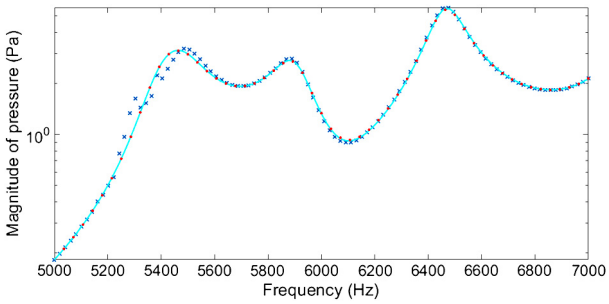

Fig. 18. Frequency evolution of the pressure magnitude (from the cut-off frequency) in one point within a rigid duct submitted to the mode $(1, 1)$ and ended by a porous layer: $(\times)$ WFE method + equivalent impedance; $(-)$ WFE method + FE boundary; $(.)$ FE method.

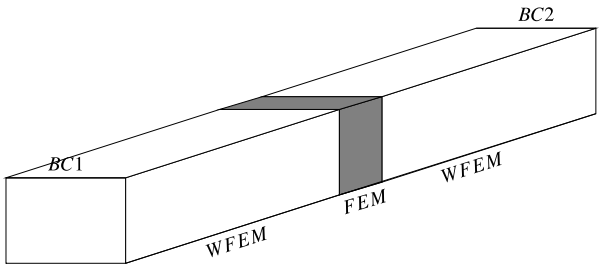

Fig. 19. Description of the approach used for the study of scattering by a porous layer inside an acoustical waveguide.

4. Conclusion

The WFE method has been used in this work for the characterisation of acoustically guided propagation and scattering. First, the frequency response of rigid ducts ended by a locally reacting lining under a prescribed pressure excitation has been calculated, and scattering inside ducts with a locally reacting lined part has been studied. Relevance of the WFE approach in terms of results accuracy has been shown while compared to the conventional approaches, i.e. either analytical or FE methods. Within the numerical validations, the wave propagation characteristics and conversion between modes with the same circumferential order for lined ducts have been highlighted. Some typical parametric studies were presented to evaluate the effect of the geometric properties of the micro-perforated plates on acoustic power attenuation and transmission loss. Then, reflection and scattering due to porous layers inside ducts were studied, and the WFE calculations of forced responses were validated by the FE method. A three-dimensional FE modelling of the porous material was combined with a WFE discretisation of the rigid parts, allowing a fast computation of the pressure anywhere inside the rigid waveguide parts. The cumbersome full FE modelling of the whole waveguide could therefore be avoided. Furthermore, it has been shown that the scattered acoustic quantities to the rigid parts can be accurately predicted without the need of an explicit representation of modes inside the lined region. The proposed approach has allowed all modes orders to be fully studied using a 3D and multi-modal approach. Although the methodology presented in this paper could serve as an interesting guideline, we think that it would be worth extending the formulation to convective propagation cases for more realistic simulations with the consideration of a convected wave equation and impedance models integrating the flow.

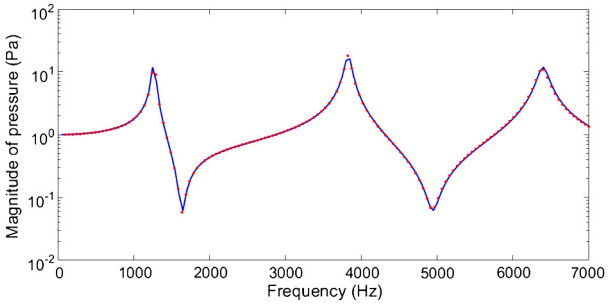

Fig. 20. Frequency evolution of the pressure magnitude in one point within a duct submitted to the mode $(0,0)$ at both ends : (–) WFE method; (.) FE method.

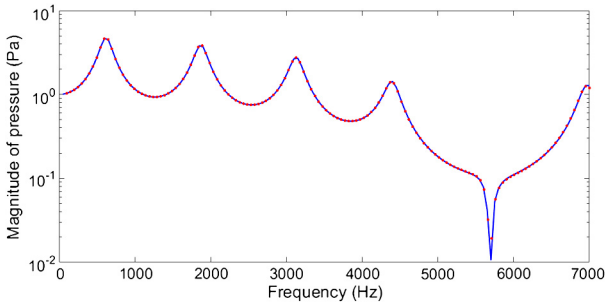

Fig. 21. Frequency evolution of the pressure magnitude in one point within a duct submitted to the mode $(0,0)$ and ended by a rigid wall: (–) WFE method; (.) FE method.

Appendix A. Dynamic condensation and boundary condition expression for porous terminations

Let us consider a periodic rigid duct filled with air with a porous layer termination at its right end. The porous material layer is backed by a rigid wall. The rigid duct part is divided into N segments. An equivalent fluid is used for modelling the porous material. The continuity of pressures and velocities vectors at the interface air–equivalent fluid provides the following relation:

$$\begin{pmatrix} \boldsymbol{\phi}_{\mathbf{p}}^{\text{inc}}\,\mathbf{Q}^{\,\text{inc}(N+1)} + \boldsymbol{\phi}_{\mathbf{p}}^{\text{ref}}\,\mathbf{Q}^{\,\text{ref}(N+1)} \\ \boldsymbol{\phi}_{\mathbf{v}}^{\text{inc}}\,\mathbf{Q}^{\,\text{inc}(N+1)} + \boldsymbol{\phi}_{\mathbf{v}}^{\text{ref}}\,\mathbf{Q}^{\,\text{ref}(N+1)} \end{pmatrix} = \begin{pmatrix} \boldsymbol{p}_{\text{l}} \\ -\boldsymbol{v}_{\text{l}} \end{pmatrix} \tag{43}$$

where superscript (i) refers to the ith cross section of the rigid duct part, and $\boldsymbol{p}_{\text{l}}$ and $\boldsymbol{v}_{\text{l}}$ are pressures and velocities vectors corresponding to the left surface of the equivalent fluid. The following equation can be then written as:

$$\boldsymbol{D}^{*}(\boldsymbol{\phi}_{\mathbf{p}}^{\text{inc}}\,\mathbf{Q}^{\,\text{inc}(N+1)} + \boldsymbol{\phi}_{\mathbf{p}}^{\text{ref}}\,\mathbf{Q}^{\,\text{ref}(N+1)}) = -(\boldsymbol{\phi}_{\mathbf{v}}^{\text{inc}}\,\mathbf{Q}^{\,\text{inc}(N+1)} + \boldsymbol{\phi}_{\mathbf{v}}^{\text{ref}}\,\mathbf{Q}^{\,\text{ref}(N+1)}) \tag{44}$$

where $\boldsymbol{D}^{*}$ is the dynamic stiffness matrix of the equivalent fluid condensed onto its left side.

A relation between amplitudes $\mathbf{Q}^{\,\text{ref}(1)}$ and $\mathbf{Q}^{\,\text{inc}(1)}$ can be then expressed:

$$\boldsymbol{\Lambda}^{-N}\,\mathbf{Q}^{\,\text{ref}} = -(\boldsymbol{D}^{*}\boldsymbol{\phi}_{\mathbf{p}}^{\text{ref}} + \boldsymbol{\phi}_{\mathbf{v}}^{\text{ref}})^{-1}(\boldsymbol{D}^{*}\boldsymbol{\phi}_{\mathbf{p}}^{\text{inc}} + \boldsymbol{\phi}_{\mathbf{v}}^{\text{inc}})\boldsymbol{\Lambda}^{N}\,\mathbf{Q}^{\,\text{inc}(1)} \tag{45}$$

with $\boldsymbol{\Lambda}$ is the diagonal matrix of eigenvalues corresponding to the incident modes.

Eq. (45) is combined with an equation resulting from the expression of the boundary condition at the left end of the duct so that $\mathbf{Q}^{\,\text{inc}(1)}$ and $\mathbf{Q}^{\,\text{ref}(1)}$ can be then easily determined by resolution of the system.

References

[1] J.O. Vasseur, P.A. Deymier, M. Beaugeois, Y. Pennec, B. Djafari-Rouhani, D. Prevost, Experimental observation of resonant filtering in a two-dimensional phononic crystal waveguide, Z. Kristallogr. Cryst. Mater. 220 (9–10) (2005) 829–835.
[2] L. Brillouin, Wave Propagation in Periodic structures, Electric Filters and Crystal Lattices, Dover Publications, London, 1946.
[3] W.X. Zhong, F.W. Williams, On the direct solution of wave propagation for repetitive structures, J. Sound Vib. 181 (3) (1995) 485–501.
[4] D. Duhamel, B.R. Mace, M.J. Brennan, Finite element analysis of the vibrations of waveguides and periodic structures, J. Sound Vib. 294 (1–2) (2006) 205–220.
[5] M.N. Ichchou, F. Bouchoucha, M.A. Ben Souf, O. Dessombz, M. Haddar, Stochastic wave finite element for random periodic media through first-order perturbation, Comput. Methods Appl. Mech. Eng. 200 (41–44) (2011) 2805–2813.
[6] O. Bareille, M. Kharrat, W. Zhou, M.N. Ichchou, Distributed piezoelectric guided-t-wave generator, design and analysis, Mechatronics 22 (5) (2012) 544–551.

[7] J. Renno, B.R. Mace, On the forced response of waveguides using the wave and finite element method, J. Sound Vib. 329 (26) (2010) 5474–5488.
[8] L. Houillon, M.N. Ichchou, L. Jezequel, Wave motion in thin-walled structures, J. Sound Vib. 281 (3–5) (2005) 483–507.
[9] J.-M. Mencik, M.N. Ichchou, Multi-mode propagation and diffusion in structures through finite elements, Eur. J. Mech. A, Solids 24 (5) (2005) 877–898.
[10] B.R. Mace, D. Duhamel, M.J. Brennan, L. Hinke, Finite element prediction of wave motion in structural waveguides, J. Acoust. Soc. Amer. 117 (5) (2005) 2835–2843.
[11] J.-M. Mencik, M.N. Ichchou, Wave finite elements in guided elastodynamics with internal fluid, Int. J. Solids Struct. 44 (7–8) (2007) 2148–2167.
[12] Y. Waki, B.R. Mace, M.J. Brennan, Free and forced vibrations of a tyre using a wave finite element approach, J. Sound Vib. 323 (3–5) (2009) 737–756.
[13] Q. Serra, M.N. Ichchou, J.-F. Deu, Wave properties in poroelastic media using a wave finite element method, J. Sound Vib. 335 (2015) 125–146.
[14] Y. Waki, B.R. Mace, M.J. Brennan, Numerical issues concerning the wave and finite element method for free and forced vibrations of waveguides, J. Sound Vib. 327 (1–2) (2009) 92–108.
[15] Y. Fan, M. Collet, M. Ichchou, L. Li, O. Bareille, Z. Dimitrijevic, Energy flow prediction in built-up structures through a hybrid finite element/wave and finite element approach, Mech. Syst. Signal Process. 66–67 (2016) 137–158.
[16] E. Manconi, Modelling Wave Propagation in Two-Dimensional Structures Using a Wave/Finite Element Technique, PhD thesis, University of Parma, Italy, 2008.
[17] D. Chronopoulos, B. Troclet, M. Ichchou, J.-P. Lainé, A unified approach for the broadband vibroacoustic response of composite shells, Composites, Part B: Eng. 43 (4) (2012) 1837–1846.
[18] M.A. Ben Souf, M.N. Ichchou, O. Bareille, M. Haddar, On the dynamics of uncertain coupled structures through a wave based method in mid- and high-frequency ranges, Comput. Mech. 52 (4) (2013) 849–860.
[19] M. Abom, Measurement of the scattering matrix of acoustical two-ports, Mech. Syst. Signal Process. 5 (2) (1991) 89–104.
[20] W.P. Bi, V. Pagneux, D. Lafarge, Y. Auregan, Modelling of sound propagation in a non-uniform lined duct using a multi-modal propagation method, J. Sound Vib. 289 (4–5) (2006) 1091–1111.
[21] W.P. Bi, V. Pagneux, D. Lafarge, Y. Auregan, Characteristics of penalty mode scattering by rigid splices in lined ducts, J. Acoust. Soc. Amer. 121 (3) (2007) 1303–1312.
[22] M. Taktak, J.M. Ville, M. Haddar, G. Gabard, F. Foucart, An indirect method for the characterization of locally reacting liners, J. Acoust. Soc. Amer. 127 (6) (2010) 3548–3559.
[23] A. Kessentini, M. Taktak, M.A. Ben Souf, O. Bareille, M.N. Ichchou, M. Haddar, Computation of the scattering matrix of guided acoustical propagation by the wave finite element approach, Appl. Acoust. 108 (2016) 92–100.
[24] A.W. Guess, Calculation of perforated plate liner parameters from specified acoustic resistance and reactance, J. Sound Vib. 40 (1) (1975) 119–137.
[25] T.H. Melling, The acoustic impedance of perforates at medium and high sound pressure levels, J. Sound Vib. 29 (1) (1973) 1–65.
[26] D. Maa, Potential of microperforated panel absorber, J. Acoust. Soc. Amer. 104 (5) (1998) 2861–2866.
[27] J.M. Renno, B.R. Mace, On the forced response of wave guides using the wave and finite element method, J. Sound Vib. 329 (26) (2010) 5474–5488.
[28] J.F. Allard, N. Atalla, Propagation of Sound in Porous Media: Modelling Sound Absorbing Materials, John Wiley Sons, 2009.
[29] Y. Yasuda, S. Uenoy, H. Sekine, A note on applicability of locally-reacting boundary conditions for Delany–Bazley type porous material layer backed by rigid wall, Acoust. Sci. Technol. 36 (5) (2015) 459–462.
[30] Y. Auregan, A. Starobinski, Determination of acoustical energy dissipation/production potentially from the acoustical transfer functions of a multiport, Acta Acust. Acust. 85 (1999) 788–792.
[31] B.S. Howard, S. Cazzolato, Acoustic Analyses Using MATLAB and ANSYS, Taylor & Francis Group, 2014.